



Minerva Access is the Institutional Repository of The University of Melbourne

Author/s:

Luo, B;Luo, D;Xiao, C;Chen, D;Simmonds, I;Zhang, X;Li, S;Zhang, W;Shi, J;Diao, Y

Title:

Recent Accelerated Decadal Shift in Winter North American Temperature Patterns Under Pacific-Atlantic Decadal Variability

Date:

2025-10-01

Citation:

Luo, B., Luo, D., Xiao, C., Chen, D., Simmonds, I., Zhang, X., Li, S., Zhang, W., Shi, J. & Diao, Y. (2025). Recent Accelerated Decadal Shift in Winter North American Temperature Patterns Under Pacific-Atlantic Decadal Variability. *Earth S Future*, 13 (10), <https://doi.org/10.1029/2025EF006006>.

Persistent Link:

<https://hdl.handle.net/11343/369624>

License:

[cc-by](#)

Earth's Future

RESEARCH ARTICLE

10.1029/2025EF006006

Key Points:

- Recent winter temperature shows a faster decadal shift between Warm West-Cold East (WWCE) and Cold West-Warm East (CWWE) patterns during 1990–2022 than during 1950–1989
- The Warm West-Cold East and Cold West-Warm East dipoles are mainly caused by North Pacific blocking events
- The PDO variability under anthropogenic warming and the positive phase of AMO can lead to the decadal variability of the WWCE (CWWE) dipole

Supporting Information:

Supporting Information may be found in the online version of this article.

Correspondence to:

B. Luo, D. Luo and C. Xiao,
luobh@tea.ac.cn;
ldh@mail.iap.ac.cn;
cdxiao@bnu.edu.cn

Citation:

Luo, B., Luo, D., Xiao, C., Chen, D., Simmonds, I., Zhang, X., et al. (2025). Recent accelerated decadal shift in winter North American temperature patterns under Pacific-Atlantic decadal variability. *Earth's Future*, 13, e2025EF006006. <https://doi.org/10.1029/2025EF006006>

Received 18 JAN 2025

Accepted 2 OCT 2025

Author Contributions:

Conceptualization: Binhe Luo

Data curation: Binhe Luo

Formal analysis: Binhe Luo

Funding acquisition: Binhe Luo,

Dehai Luo, Cunde Xiao, Ian Simmonds

Investigation: Binhe Luo

Methodology: Binhe Luo, Dehai Luo

Project administration: Binhe Luo,

Dehai Luo, Cunde Xiao, Ian Simmonds

Resources: Binhe Luo, Dehai Luo

Software: Binhe Luo

© 2025. The Author(s).

This is an open access article under the terms of the [Creative Commons Attribution License](https://creativecommons.org/licenses/by/4.0/), which permits use, distribution and reproduction in any medium, provided the original work is properly cited.

Recent Accelerated Decadal Shift in Winter North American Temperature Patterns Under Pacific-Atlantic Decadal Variability

Binhe Luo¹, Dehai Luo^{2,3} , Cunde Xiao¹ , Deliang Chen⁴ , Ian Simmonds⁵ , Xiangdong Zhang⁶ , Shujun Li^{7,8} , Wenqi Zhang⁹, Jiaqi Shi^{2,3} , and Yina Diao¹⁰ 

¹State Key Laboratory of Earth Surface Processes and Disaster Risk Reduction, Beijing Normal University, Beijing, China, ²State Key Laboratory of Earth System Numerical Modeling and Application, Institute of Atmospheric Physics, Chinese Academy of Science, Beijing, China, ³University of Chinese Academy of Sciences, Beijing, China, ⁴Department of Earth System Sciences, Tsinghua University, Beijing, China, ⁵School of Geography, Earth and Atmospheric Sciences, University of Melbourne, Parkville, VIC, Australia, ⁶North Carolina State University, Asheville, NC, USA, ⁷State Key Laboratory of Physical Oceanography/Frontiers Science Center for Deep Ocean Multispheres and Earth System, Ocean University of China, Qingdao, China, ⁸Laoshan Laboratory, Qingdao, China, ⁹Center for Monsoon System Research, Institute of Atmospheric Physics, Chinese Academy of Sciences, Beijing, China, ¹⁰College of Oceanic and Atmospheric Sciences, Ocean University of China, Qingdao, China

Abstract Global warming and internal climate variability have changed winter temperature extreme regimes in North America, affecting droughts and wildfires in the western United States. However, how internal climate variability influences North American winter temperature extreme patterns remains poorly understood. Here, we demonstrate that the recent winter North American surface air temperature (SAT) exhibits an accelerated decadal alternation between Warm West-Cold East (WWCE) and Cold West-Warm East (CWWE) dipoles because their variations show shorter decadal periods during 1990–2022 than during 1950–1989 and are regulated by the Pacific Decadal Oscillation (PDO) variability. While the winter WWCE dipole mainly linked to North Pacific blocking events exhibited a smaller mean amplitude during 1990–2022 than 1950–1989 due to the weakened positive PDO phase during 1990–2022 under the positive phase of the Atlantic Multidecadal Oscillation (AMO), the winter CWWE showed a larger mean amplitude during 1990–2022 due to the stronger negative PDO phase than during 1950–1989. Our results further suggest that the recent rapid decadal shift of North American winter temperatures is primarily attributed to the PDO variability likely due to anthropogenic warming under the positive AMO.

Plain Language Summary The North American winter surface air temperature (SAT) pattern exhibits a more rapid decadal transition between Warm West-Cold East (WWCE) and Cold West-Warm East (CWWE) dipoles during 1990–2022 than during 1950–1989. These decadal variations seem to have a footprint of the Pacific Decadal Oscillation (PDO) variability with shortened periods in recent decades likely due to anthropogenic warming. While the sub-seasonal WWCE and CWWE dipoles are produced by North Pacific blocking events, the rapid decadal alternation between the positive and negative phases of PDO during 1990–2022 under the positive phase of AMO can lead to an accelerated decadal alternation between the winter WWCE and CWWE dipoles, as a result of the winter mean effect of sub-seasonal WWCE and CWWE dipoles, by regulating North Pacific blocking events. The obtained results are of great significance for understanding the variability and physical cause of North American temperature extreme patterns, droughts and wildfires under greenhouse warming.

1. Introduction

In recent decades, North America has experienced many extreme cold weather events (Smith & Sheridan, 2018; Vavrus et al., 2006; Walsh et al., 2001), although it is not clear whether their number is increasing (Cohen et al., 2023). Tens of millions of people in the region have been seriously affected by extremely low temperatures and heavy snowfalls associated with these events. Examples of these episodes occurred in 2013/2014 and 2014/2015 (Hartmann, 2015; Peng et al., 2019; Yu & Zhang, 2015). Many studies have suggested that North American winter cold extremes are significantly influenced by atmospheric teleconnection patterns associated with North Pacific (Ge & Luo, 2023a, 2023b; Kushnir & Lau, 1992; Pitcher et al., 1988) and North Atlantic (Veres &

Supervision: Binhe Luo, Dehai Luo, Deliang Chen, Ian Simmonds, Xiangdong Zhang

Validation: Binhe Luo, Dehai Luo, Shujun Li, Wenqi Zhang, Jiaqi Shi, Yina Diao

Visualization: Binhe Luo, Wenqi Zhang

Writing – original draft: Binhe Luo

Writing – review & editing: Binhe Luo, Dehai Luo, Deliang Chen, Ian Simmonds, Xiangdong Zhang, Wenqi Zhang

Hu, 2015) sea surface temperature (SST) anomalies and the effect of diminishing sea ice in the west of Greenland (Lee et al., 2015; R. Zhang et al., 2022; W. Zhang et al., 2022; X. Zhang et al., 2022). However, how the internal variability from the North Pacific and North Atlantic in a warming climate influences the occurrence and variability of North American winter cold extreme patterns is not well understood. Therefore, investigating the mechanisms leading to the occurrence and variability of winter cold extremes or low temperatures over North America is crucial for better understanding and more accurately predicting extreme cold events. This has significant implications for mitigating impacts on human life, socio-economics and ecosystem, and for managing summer wildfires (Considine, 2000; Ladwig et al., 2016; Liu et al., 2023).

Prominent features of the winter surface air temperature (SAT) over North America are the Warm West-Cold East (WWCE) and warm Arctic-cold North American continent (WACNA) dipole patterns (Kug et al., 2015; Overland et al., 2011; Singh et al., 2016). The winter WWCE dipole, associated with the Pacific-North American pattern (PNA), North Pacific Oscillation (NPO), North Pacific blocking (PB) and North Atlantic Oscillation (NAO) events (Lin, 2015; Luo et al., 2020; Vigaud et al., 2018; Yu et al., 2016), shows a cold anomaly in the Eastern United States and a warm anomaly in the Western United States. The winter SAT also exhibits a marked interannual-interdecadal variability under the modulation of El Niño-Southern Oscillation (ENSO), Victoria mode, Pacific Decadal Oscillation (PDO), and Atlantic Multidecadal Oscillation (AMO) (Dai, 2013; Ji et al., 2024; McCabe et al., 2004; Wang et al., 2014).

The winter WWCE pattern has been shown to be a main contributor to the drought over California (Kushnir & Lau, 1992; Mo et al., 2009), in addition to the contribution of anthropogenic forcing (R. Zhang et al., 2022; W. Zhang et al., 2022; X. Zhang et al., 2022; Zhuang et al., 2021). The formation of the WWCE dipole is mainly due to a persistent high-pressure ridge on the West Coast of North America with a trough in eastern North America (Swain et al., 2016; Wang et al., 2017; R. Zhang et al., 2022; W. Zhang et al., 2022; X. Zhang et al., 2022). The Western United States is a fire-prone region where extensive and high-intensity wildfires can occur (Abolafia-Rosenzweig et al., 2022; Zhuang et al., 2021; Zou et al., 2021). However, large wildfire risk is recently increasing in the Eastern United States with a seasonal shift to an earlier time during 2011–2020 (Donovan et al., 2023). The increasing frequency of large wildfires in the Eastern United States is likely due to persistent warm winters there via enhancing winter vapor pressure deficits (Abolafia-Rosenzweig et al., 2022).

Based on the above physical discussion, we form the hypothesis that the WWCE has likely weakened and changed its phase from positive to negative with a cold west-warm east (CWWE) dipole structure during the recent decade. In this study, we test this hypothesis and explore the potential associated mechanisms by examining the role of internal variability (e.g., PDO and the AMO) with a focus on the responses of the occurrence of PB events. This will reveal the different roles of the internal PDO and AMO variations in producing the decadal-interdecadal variability of the winter SAT anomalies over North America. On this basis, a new result is presented that the winter North American temperature pattern shows an accelerated decadal alternation between the WWCE and CWWE dipoles from 1950–1989 to 1990–2022.

2. Data and Methods

2.1. Data

We used the daily data on a $1^{\circ} \times 1^{\circ}$ grid for winter (December, January and February, DJF) for the period from December 1950/February 1951 to December 2022/February 2023 (1950–2023 hereafter) taken from the ERA5 reanalysis of European Centre for Medium-Range Weather Forecasts (ECMWF) (Hersbach et al., 2020) and the ERA5-Land for Medium-Range Weather Forecasts (ECMWF) (Muñoz-Sabater et al., 2021). The data includes daily 500-hPa geopotential height (Z500), 500-hPa zonal wind (U500) and SAT (2m).

2.2. Empirical Orthogonal Function (EOF) Analysis and Decadal-Interdecadal Modes

Empirical Orthogonal Function (EOF) analysis of the linearly detrended DJF-mean SAT anomalies, performed in the North American region (25° – 70° N, 140° – 60° W) during the 1950–2022, is used to extract the first and second EOF modes (EOF1 and EOF2) of the winter North America SAT anomaly and their corresponding principal components (PC1 and PC2) by computing the eigenvectors of a spatially weighted anomaly covariance matrix. A 9–30-year (or 9–30-yr) band-pass filter of PC1 is used to represent the decadal variability of the North American

SAT EOF1 mode via the Lanczos method (Emery & Thomson, 2004), whereas a 30-year (or 30-yr) low-pass filter of PC2 is used to represent the interdecadal variation of the EOF2 mode.

2.3. Time Series of Winter PDO and AMO Indices

The PDO index used in this study is taken from NOAA (<https://www.ncei.noaa.gov/access/monitoring/pdo/>), while the AMO index is taken from Koninklijk Nederlands Meteorologisch Instituut (KNMI) Climate Explorer (<http://climexp.knmi.nl/selectindex.cgi?id=someone@somewhere>). Here, we define the positive (negative) PDO winter based on the value with >0 (<0) of a 9–30-year band-pass filtered DJF-mean PDO index, whereas the positive (negative) AMO winter is based on the value with >0 (<0) of a 30-year low-pass filtered DJF-mean AMO index. The PDO (AMO) index with a 9–30-year band-pass (30-year low-pass) filtering represents its decadal (interdecadal) variation based on the Lanczos method (Emery & Thomson, 2004).

2.4. Regression Analysis

The regressed fields of detrended SAT and Z500 anomalies against the normalized time series of the SAT PC1, PC2, PDO, and AMO are derived in terms of a linear regression equation:

$$Y = a + bX \quad (1)$$

where Y is a predicated variable, a is the error term, the matrix X are independent variables and b is the regression coefficient.

2.5. Identification of North Pacific Blocking (PB) Events

To extract PB events, we identify such events occurring in the longitudinal sector from 160°W – 100°W , based on the one-dimensional blocking index of Tibaldi and Molteni (1990) (TM hereafter). The TM index is defined in terms of the reversal of the meridional gradient of Z500:

$$\text{GHGN} = [Z500(\phi_N) - Z500(\phi_o)] / (\phi_N - \phi_o) \quad (2a)$$

$$\text{GHGS} = [Z500(\phi_o) - Z500(\phi_S)] / (\phi_o - \phi_S), \quad (2b)$$

at the three given reference latitudes: $\phi_N = 80^{\circ}\text{N} + \Delta$, $\phi_o = 60^{\circ}\text{N} + \Delta$, $\phi_S = 40^{\circ}\text{N} + \Delta$ and $\Delta = -4^{\circ}, 0^{\circ}, 4^{\circ}$ in a fixed longitude. A blocking event is defined to have taken place if the conditions $\text{GHGS} > 0$ and $\text{GHGN} < -10 \text{ gpm (deg lat)}^{-1}$ hold for at least three consecutive days and are satisfied for at least one choice of Δ in a given zonal region covering at least 15° of longitude.

2.6. Data Treatment and Statistical Significance Tests

The long-term (1950–2022) mean and linear trend of all the daily or monthly data for each calendar day or month are removed to generate de-seasonalized anomaly data for the analyses and composites of atmospheric variable fields. We also used the two-sided student t -test to examine the statistical significance of the anomaly fields, and the Mann-Kendall (MK) test is also employed in this paper. These statistical methods are fully described in Wilks (2011) (Emery & Thomson, 2004).

2.7. Meridional Potential Vorticity Gradient (PV_y) Theory of Atmospheric Blocking in a Nonlinear Multiscale Interaction (NMI) Model

We used the nonlinear multiscale interaction (NMI) model of atmospheric blocking events to diagnose the spatiotemporal evolution of atmospheric blocking in terms of the background meridional potential vorticity gradient (PV_y or PV_y) (Luo et al., 2019; Luo & Zhang, 2020; Zhang & Luo, 2020). The theory shows that when PV_y is smaller, the atmospheric blocking has a weaker dispersion and a stronger nonlinearity so that it has longer lifetime, lesser eastward movement, larger zonal scale and slower decay, and vice versa (Luo et al., 2019; Zhang & Luo, 2020). Here, the non-dimensional equivalent barotropic PV_y is scaled by the characteristic velocity \tilde{U} ($\sim 10 \text{ m/s}$) and length \tilde{L} ($\sim 10^6 \text{ m}$). The non-dimensional PV_y can be expressed as

$$PV_y = \beta - \frac{\partial^2 U}{\partial y^2} + FU \quad (3)$$

where $F = \frac{\tilde{L}^2}{R_d^2}$, where $\beta = \beta_0 \tilde{L}^2 / \tilde{U}$, $U(y)$ is the non-dimensional basic zonal wind, R_d is the radius of Rossby deformation and β_0 is the meridional gradient of the Coriolis parameter at a given reference latitude φ_0 , respectively. We set $F \approx 1$ as a fixed parameter (Zhang & Luo, 2020).

3. Results

3.1. Decadal-Interdecadal Variability of North American Winter Temperature Extreme Patterns

Here, we use a linear detrending to crudely remove the direct effect of greenhouse warming trend. We then perform an EOF analysis of the detrended winter (December to February, DJF) mean SAT anomalies over North America (25°–70°N, 140°–60°W) during 1950–2022. The first mode (EOF1) with its Principal Component (PC1) explains 28% of the variance and exhibits a WWCE dipole along the zonal direction in the southern part of North America (Figure 1a) for a positive value of PC1. When PC1 is positive, this EOF1 mode reflects the decadal-interdecadal variability of North American SAT anomalies and partly includes a warm west-cold east (WWCE) dipole in the southern part of North America and a Warm Arctic-Cold North America (WACNA) dipole in the eastern part of North America (Kug et al., 2015). We see that the WWCE dipole denoted by EOF1 mode with its positive PC1 is distinct from the North American winter temperature dipole (NAWTD) pattern defined by Singh et al. (2016) based on the difference of SAT anomalies between the western and eastern parts of North America. This mode reflects that the decadal variability part of the WWCE (WACNA) dipole is mainly located in the southern (eastern) side of North America. In the study over the shorter period of 1980–2015 of Singh et al. (2016), the formation of the NAWTD pattern is associated with the presence of a wave train with zonal wavenumber 2 across North American midlatitudes (Figure 1 of Singh et al., 2016). While the NAWTD exhibits an upward trend, it does not show a notable decadal-interdecadal variability (Figure 2 of Singh et al., 2016). In the present study, we further reveal that the phases of PDO and AMO can induce the decadal-interdecadal variability of North American SAT anomalies through modulating blocking events over the northeast Pacific.

It is further found that the winter WWCE dipole in the south side of North America, as denoted by the SAT EOF1 mode, exhibits a pronounced interannual-decadal variability (Figure 1c), which is likely tied to the modulation by ENSO (R. Zhang et al., 2022; W. Zhang et al., 2022; X. Zhang et al., 2022) and PDO (Ge & Luo, 2023a, 2023b). Another interesting feature is that the PC1 time series has a longer mean decadal period of about 20 years during 1950–1989 than the shorter mean decadal period of about 14 years during 1990–2022 (Figure 1c). The mean period difference is statistically significant ($p < 0.05$) based on the Monte-Carlo test with 10,000 samples. This implies that the winter North American temperature pattern exhibits an accelerated decadal shift from 1950–1989 to 1990–2022. We also mention that the decadal variability of the EOF1 WWCE dipole amplitude depends on the sign of the PC1 time series. By construction, a positive value of PC1 represents a WWCE dipole, whereas its negative value characterizes a cold west-warm east (CWWE) dipole in the North American midlatitudes. The PC1 has a mean negative value of -0.26 (-0.32), and a mean positive value of 0.43 (0.37) over 1950–1989 (1990–2022), even though its two large negative values exceed -2.0 during 1950–1989. This suggests that the mean CWWE (WWCE) dipole is stronger (weaker) during 1990–2022 than during 1950–1989, thus implying that the winter North American SAT WWCE dipole has exhibited a decadal weakening at a rate of about 14% from 1950–1989 to 1990–2022, whereas the CWWE dipole has undergone a decadal intensifying at a rate of about 23% during the same period. These mean amplitude differences between 1990–2022 and 1950–1989 are also statistically significant ($p < 0.05$ in the Monte-Carlo test). We mention that in order to ascertain whether our findings here are influenced by the linear detrending we have employed, we recalculated these results after performing the detrending with a second order polynomial. The results were essentially unaffected (Figure S2 in Supporting Information S1). EOF2, which explains about 19% of the variance, shows a widespread negative SAT anomaly over the whole North America (Figure 1b). The North test confirms that EOF1 and EOF2 are statistically distinguishable (North et al., 1982).

To further extract the decadal (interdecadal) variation of the SAT EOF1 (EOF2) mode over North America, we apply the 9–30-year (or 9–30-yr) band-pass and 30-year (or 30-yr) low-pass filters to the PC1 and PC2 time series over 1950–2022, respectively. The regressed winter 500-hPa geopotential height (Z500) and SAT anomalies onto

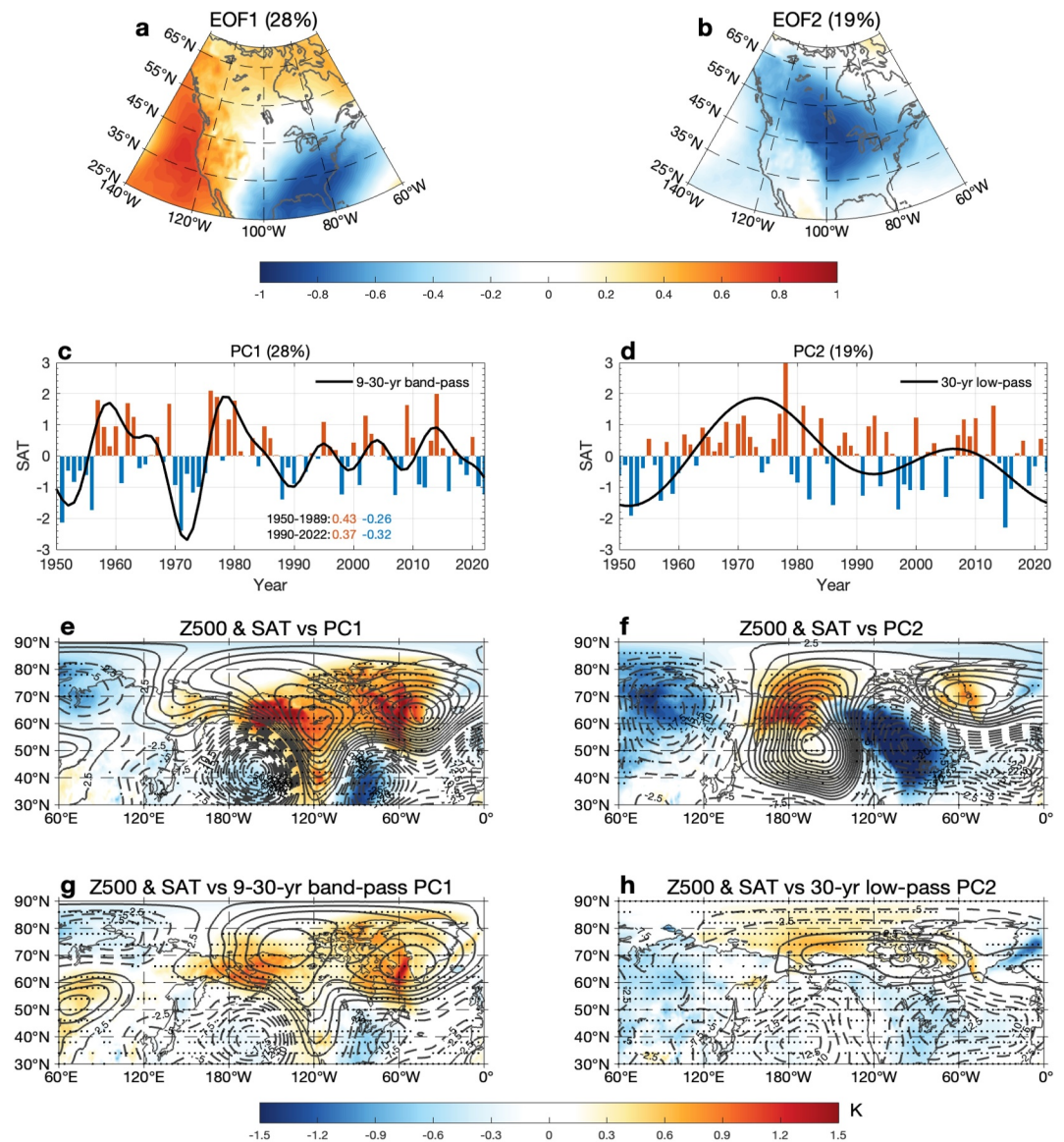


Figure 1. Spatial structure and variability of winter North American surface air temperature (SAT) of the leading and second empirical orthogonal function (EOF1 and EOF2) modes of winter SAT anomalies during 1950–2022 and regressed atmospheric fields onto the time series of their principal components (PC1 and PC2) without and with low-pass filtered curves. (a, b) Spatial patterns of first and second leading empirical orthogonal function (EOF1 and EOF2) modes of linearly detrended winter (December to February, DJF) mean surface air temperature (SAT) anomaly over North America (25°–70°N, 140°–60°W) and (c, d) their corresponding normalized principal components (PC1 and PC2). (e–h) Regressed DJF-mean 500-hPa geopotential height (Z500, contours, CI = 2.5 gpm) and SAT (color shading, in K) anomalies against the normalized (e, f) unfiltered PC1 and PC2, (g) 9–30-year (or 9–30-yr) band-pass PC1 (black line) and (h) 30-year (or 30-yr) low-pass PC2 (black line) time series during 1950–2022, where the black dot represents the color shading region being above the 95% confidence level for a two-sided Student's *t*-test. In panel c, the red (blue) number represents the mean of the positive (negative) PC1 value averaged over 1950–1989 (1990–2022).

the 9–30-year bandpass filtered PC1 time series show that the winter WWCE dipole on decadal timescales is accompanied by a high latitude PB-like anticyclone in the northeast Pacific and a winter negative NAO (NAO⁻)-like pattern with their anticyclonic centers being near the North American continent for a positive PC2 (Figure 1g). While the SAT EOF2 mode exhibits a marked interannual variability (Figures 1d and 1f) associated with ENSO (R. Zhang et al., 2022; W. Zhang et al., 2022; X. Zhang et al., 2022), it also possesses an interdecadal variability (Figure 1h) tied to an anticyclonic anomaly located in the North American Arctic region (Figure 1f).

We note that the cold anomaly of the 30-year low-pass filtered SAT EOF2 pattern is located in the central-eastern North America for a positive PC2 (Figure 1h), even though it is much weaker than that of the unfiltered pattern (Figure 1f). Because the PC2 time series shows less notable decadal variability (Figure 1d), the strong cold anomaly of the SAT EOF2 mode over the whole North America mainly consists of interannual and interdecadal parts.

As noted by Ge and Luo (2023b), the anticyclonic (or positive Z500) anomalies in the mid-high latitudes of North Pacific are mainly modulated by the ENSO and PDO. Thus, when the timescales less than 30 years are filtered out, the interdecadal variability longer than 30 years becomes much weaker so that the positive Z500 anomalies longer than 30 years are almost absent in the middle latitudes of the eastern Pacific, even though positive Z500 anomalies appear in high latitudes. As a result, the cold anomalies are relatively weak across the North America and are found mainly in the central-eastern North America (Figure 1h). Therefore, the weak cold anomalies in the central-eastern North America mainly reflect the interdecadal variability of the North American SAT anomalies induced by AMO, while major parts of the cold anomaly in Figure 1f are an interannual signal (Figure 1d). On the other hand, we can see that the interdecadal cold anomaly does not appear in the western part of the North American midlatitudes. Thus, it is likely that the AMO can contribute to the WWCC dipole on decadal-interdecadal timescales in the North American midlatitudes through producing weak interdecadal cold anomalies in the central-eastern North America (Figure 1h).

To verify the robustness of our results, we performed an EOF analysis using the ERA5-Land data, which includes only land grid points (Figure S1 in Supporting Information S1). It is interesting to see that the first and second EOF modes (EOF1 and EOF2) obtained from ERA5 and ERA5-Land data sets are very similar in spatial structure and temporal variability, although their first and second principal components (PC1 and PC2) are reversed. Specifically, the EOF1 (EOF2) pattern in the ERA5 data closely matches the EOF2 (EOF1) pattern in the ERA5-Land data. A strong agreement between the two data sets confirms that the dominant modes of the SAT variability over North America are robust and not sensitive to the inclusion of oceanic grid points.

3.2. Footprint of the Anthropogenic Warming-Induced PDO Variability in the Decadal Variability of the North American Zonal Air Temperature Dipole

To explore in detail the potential drivers for these changes, we show in Figures 2a and 2b the DJF-mean PDO and AMO indices over 1950–2022. We find that the DJF-mean PDO index displays a longer (shorter) decadal period of about 20 (14) years on average over 1950–1989 (1990–2022) (Figure 2a), with periods consistent with those of the SAT PC1 time series in the two sub-periods (Figure 1c). The PDO index has a mean of the positive values of 0.45 (0.38) over 1950–1989 (1990–2022), and a mean negative value of -0.20 (-0.48) over 1950–1989 (1990–2022). Clearly, the positive (negative) phase of PDO shows a decadal weakening (intensifying) at a rate of about 16% (140%) in amplitude from 1950–1989 to 1990–2022. As noted in previous studies (Fang et al., 2014; Geng et al., 2019; Zhang & Delworth, 2016), the lifespan of the PDO is largely shortened due to the greenhouse warming-induced intensification of oceanic stratification (Fang et al., 2014; Zhang & Delworth, 2016) via the increased propagation speed of oceanic Rossby waves (Saenko, 2006). Global warming is significantly enhanced after 1990, and as a consequence we expect to see the shortened lifetime of the PDO after this time. However, we find that the PDO amplitude suppression during 1990–2022 occurs only for its positive phase, whereas the negative PDO is intensified from 1950–1989 to 1990–2022. The same PDO amplitude variability signal can also be seen in the SAT PC1 time series (Figure 1c). In addition, because the predictability of the PDO is reduced under anthropogenic warming (Li et al., 2020), one could infer that the North American SAT WWCE or CWWE dipole will become less predictable in a warming climate. Thus, the effect of the anthropogenic warming trend still persists in the decadal variability of the North American zonal temperature dipole via the PDO variability, even though the direct effect of anthropogenic warming trend has been crudely removed. To some extent, the two phases of PDO also have a strong asymmetric impact on the North American air temperature patterns on decadal timescales.

We see that the positive PDO phase (PDO⁺) favors the WWCE dipole through the formation of a winter PB-like pattern (Figure 2c), though the winter NAO⁻-like pattern is very weak. In contrast, the CWWE dipole is easily formed in North America in the negative phase of PDO. This suggests that the shift of PDO from the positive to negative phase is important for the decadal variability of the winter North American SAT pattern from a WWCE to CWWE. This conclusion is supported by the significant correlation of 0.72 ($p < 0.05$) between a 9–30-year

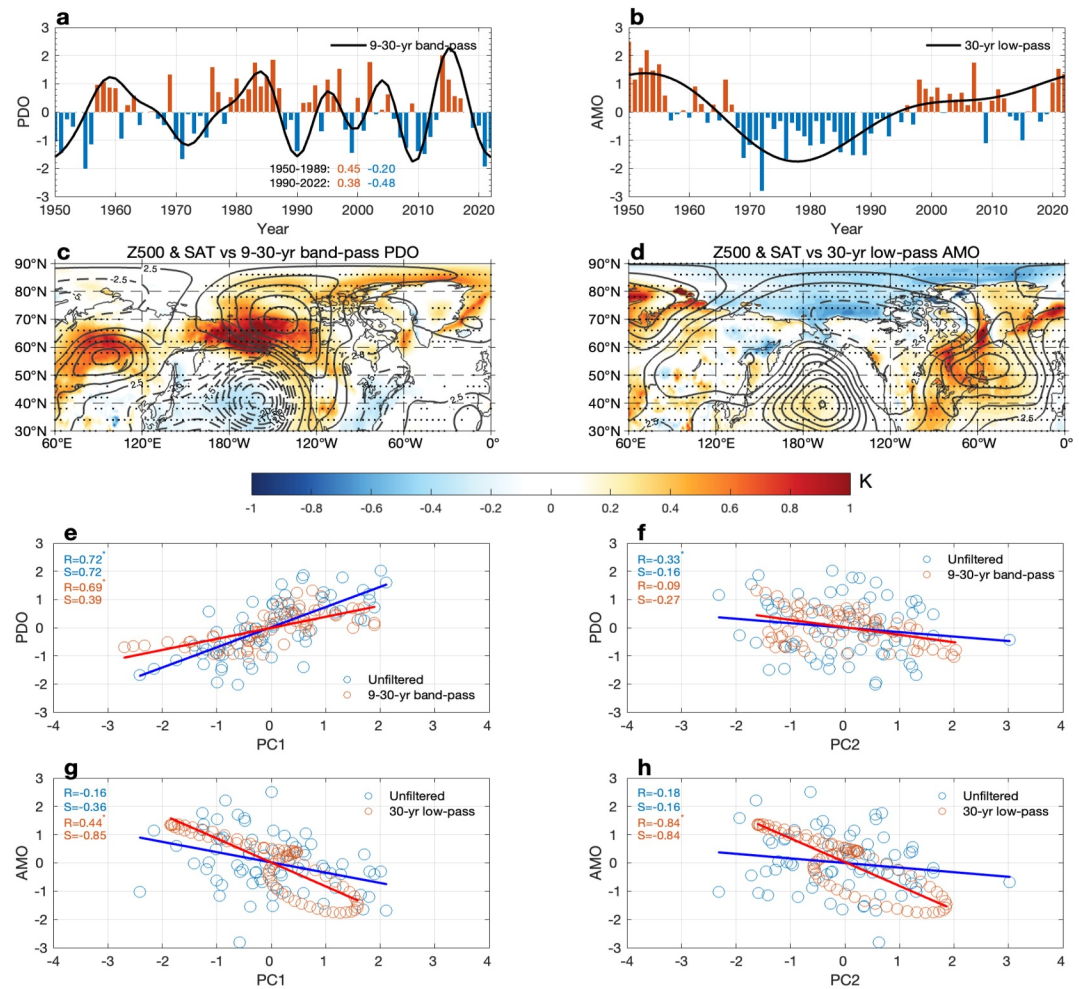


Figure 2. Temporal variations of winter Pacific Decadal Oscillation (PDO) and Atlantic Multidecadal Oscillation (AMO) indices and their relationships with the winter North American surface air temperature (SAT) regimes during 1950–2022. (a, b) Time series of normalized winter (December to February, DJF) mean (a) Pacific Decadal Oscillation (PDO) index with a 9–30-year (or 9–30-yr) band-pass curve (black line) and (b) Atlantic Multidecadal Oscillation (AMO) index with a 30-year (or 30-yr) low-pass curve (black line) during 1950–2022. (c, d) Regressed winter-mean 500-hPa geopotential height (Z500, contours, CI = 2.5 gpm) and SAT (color shading, in K) onto (c) 9–30-year band-pass PDO index and (d) 30-year low-pass AMO index. The dot represents the color shading region above the 95% confidence level for a two-sided Student's *t*-test. (e–h) Scatter diagrams of the normalized DJF-mean (e, f) PDO and (g, h) AMO time series against the normalized PC1 and PC2 time series of the DJF-mean SAT EOF1 and EOF2 modes over North America. The blue (red) circle represents the unfiltered (9–30-year band-pass or 30-year low-pass) case. The value of *R* (*S*) denotes the correlation (slope) coefficient being statistically significant for the 95% confidence (asterisk). The red (blue) numbers in (a) represent the values of the mean positive (negative) PC1 averaged over 1950–1989 and 1990–2022.

bandpass filtered PDO index and SAT PC1 (blue line in Figure 2e), even though the unfiltered PDO index has a significant correlation with the SAT PC1 (red line in Figure 2e). In addition, 9–30-year bandpass filtered SAT PC2 has a weak correlation with the PDO index (Figure 2f). This result indicates that the SAT EOF1 pattern is significantly modulated by the PDO variability. The AMO can also influence the decadal variability of the North American SAT EOF1 mode associated with PDO (Figures 2d, 2e, and 2g), even though it makes a larger contribution to the interdecadal variation of the winter SAT EOF2 mode (Figure 2h). Specially, the 30-year low-pass filtered AMO index is significantly correlated with the PC1 with a correlation coefficient of 0.44 ($p < 0.05$) (Figure 2g) and the PC2 with a correlation coefficient of 0.84 ($p < 0.05$) (Figure 2h). This result indicates that the AMO plays a dominant role in the interdecadal SAT variability over the North America.

We also find that the positive AMO phase (AMO⁺) favors a warm anomaly in eastern North America via the presence of an anticyclonic anomaly over North Atlantic midlatitudes (Figure 2d), whereas the associated winter

SAT change is relatively weak in western North America. Thus, AMO^+ suppresses the WWCE dipole and favors the CWWE dipole. In contrast, a strong cold anomaly appears in the eastern part of North America for the negative AMO phase (AMO^-) (a reversed pattern of Figure 2d), which favors the WWCE dipole and suppresses the CWWE dipole. In summary, the transition of the PDO at the 9–30-year spectral band from a positive to a negative phase during the recent decade causes a shift of the WWCE pattern to the CWWE pattern as revealed by the SAT EOF1 mode, while the AMO^+ -induced SAT anomalies strengthens the PDO⁻-driven CWWE dipole. Consequently, the recent decadal shift from the WWCE dipole to the CWWE dipole pattern is mainly associated with the PDO variability, whereas the AMO mainly induced the interdecadal variability of the SAT anomalies in the central-eastern North America.

3.3. Decadal Changes in North Pacific Blocking Events

We see that the DJF-mean SAT dipole over North America is related to the presence of a winter PB anticyclone-like pattern (Figures 1e and 2c). Thus, we consider the role of the PDO and AMO in modulating extreme cold/warm events driven by PB events in North America. Here, we classify PB events in terms of the values of the normalized time series of the 9–30-year band-pass filtered PDO and 30-year low-pass filtered AMO indices over 1950–2022. The values with <0 (>0) of the filtered PDO and AMO indices are defined as the negative (positive) phases of the PDO and AMO or PDO^- and AMO^- (PDO^+ and AMO^+). We use the TM blocking algorithm to identify PB events over the region (160° – 100° W). We found 36 PDO^- , 37 PDO^+ , 30 AMO^- and 43 AMO^+ winters during the 1950–2022 when there were 166 total PB events (Figure S3a in Supporting Information S1).

Stratification of the years reveals that there are 81 (85) PB events or 2.25 (2.30) PB events per winter for the PDO^- (PDO^+) winters (Figures S3b and S3c in Supporting Information S1). But there are 80 (84) PB events or 2.67 (1.95) PB events per winter for the AMO^- (AMO^+) winters (Figures S3d and S3e in Supporting Information S1). Clearly then, the phase of the PDO does not substantially influence the number of PB events, whereas AMO^- is more favorable for the PB events than AMO^+ . We find there to be 17 PDO^- & AMO^- , 19 PDO^- & AMO^+ , 13 PDO^+ & AMO^- , and 24 PDO^+ & AMO^+ combination winters over our period, which have in turn 53, 28, 29 and 56 PB events, corresponding to 3.1, 1.5, 2.2 and 2.3 PB events per winter, respectively (Figures S3f and S3i in Supporting Information S1). This then indicated that PDO^- can increase (decrease) PB events via the combination with AMO^- (AMO^+) because AMO^- favors more PB events than AMO^+ . Thus, the PB events are favored (suppressed) by AMO^- (AMO^+) only during the PDO^- period, even though AMO^- and AMO^+ do not influence the number of PB events in the PDO^+ period.

3.4. Combined Effect of PDO and AMO

To further reveal the evolutionary dynamics at play here, we calculate the time-mean fields of composite daily Z500 and SAT anomalies of PB events during the blocking lifecycle for different phases of PDO and AMO (Figures 3a–3d) and their four combinations (Figures 3e–3h). Correspondingly, the impact of PB events on the daily SAT anomalies in the western and eastern parts of United States are shown in Figure 4 for different combinations of PDO and AMO. We see from Figure 3 that the anticyclonic anomaly of PB has a longer lifetime, a larger zonal scale, less westward movement, and is located more eastward and in higher latitudes (Figure S4 in Supporting Information S1) for PDO^+ (Figure 3b) than for PDO^- (Figure 3a). This is because the PDO^+ is characterized by a weakening of westerly winds to the north of 60° N and a reduced meridional gradient of potential vorticity (PV_y) over the mid-high latitudes of North Pacific (Figures 5b and 5f) compared to the PDO^- (Figures 5a and 5e). As we indicated earlier, the differences of these blocking characteristics can be explained by using the PV_y theory of atmospheric blocking based on a nonlinear multiscale interaction (NMI) model in a given basic zonal wind (Figures S5 and S6 in Supporting Information S1). Because the time-mean effect of sub-seasonal WWCE dipoles in winter mostly reflects the winter WWCE dipole pattern, below we will focus on examining the sub-seasonal variability of the WWCE and CWWE dipoles in winter.

We see that PB can produce a strong sub-seasonal cold anomaly in the northwest region of North America for PDO^- (Figure 3a), whereas it can result in a relatively strong sub-seasonal WWCE dipole in the midlatitudes of North America (35° – 55° N) for PDO^+ (Figure 3b) because the anticyclonic anomaly of PB can extend southward to about 35° N, resulting in a persistent high-pressure ridge along the west coast of the United States. The southward extension of such a high ridge supports a sub-seasonal WWCE-like dipole pattern (Figure 3b), although the sub-seasonal SAT WWCE dipole pattern seems to be relatively weak during the PDO^+ & AMO^-

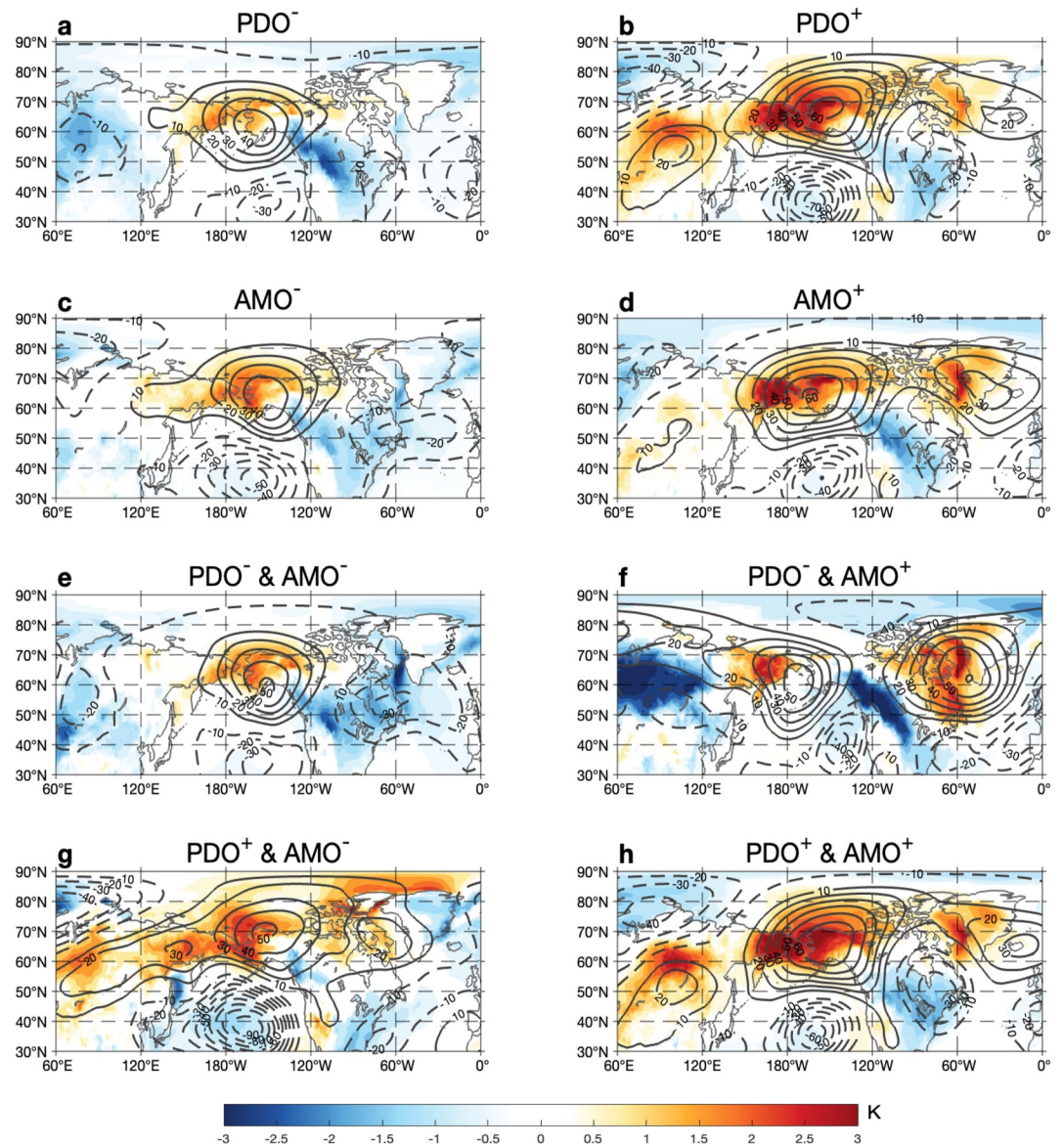


Figure 3. Time-mean composite daily 500-hPa geopotential height (Z500) and surface air temperature (SAT) anomalies during the blocking lifecycles of North Pacific blocking events. (a–h) Time-mean fields of composite daily Z500 (contours, CI = 10 gpm) and SAT (color shading, in K) anomalies averaged from lag -10 to $+10$ days of Pacific blocking (PB) events (lag 0 denotes the peak day of blocking) for the (a) negative PDO (PDO⁻), (b) positive PDO (PDO⁺), (c) negative AMO (AMO⁻), (d) positive AMO (AMO⁺) as well as their different combinations of (e) PDO⁻ & AMO⁻, (f) PDO⁻ & AMO⁺, (g) PDO⁺ & AMO⁻ and (h) PDO⁺ & AMO⁺. The negative (positive) PDO or AMO phase is defined in terms of <0 (>0) standard deviations (STDs) of the normalized 9–30-year band-pass winter (December to February, DJF) mean PDO or 30-year low-pass winter mean AMO index. The color shading indicates the region with the SAT anomalies being significant with a 95% confidence level based on a two-sided Student's *t*-test.

(Figure 3e). Therefore, a sub-seasonal WWCE dipole is favored to form over North America due to the presence of PB events under the PDO⁺ condition. For AMO⁻, a weak widespread cold anomaly associated with PB events appears over North America (Figure 3c). However, a sub-seasonal WWCE dipole, albeit weak, is also seen for AMO⁺ (Figure 3d). Thus, the phase of AMO appears to modulate the sub-seasonal WWCE dipole regimes over North America produced by PB events, even under the PDO⁺ condition.

Our analysis further demonstrates that while the PB events are most frequent for the PDO⁻ & AMO⁻ in the four combinations, the PB is short-lived (Figure 5) in this case because PV_y is relatively large (Figure 6). Even so, a

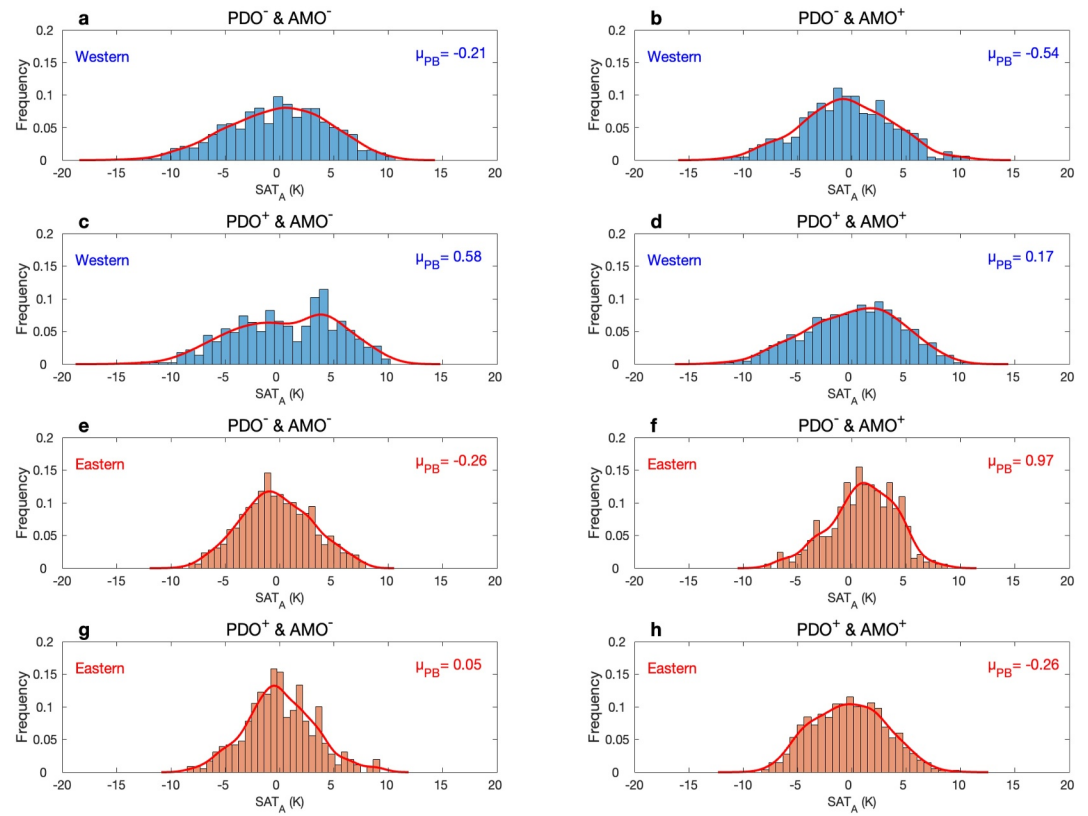


Figure 4. Probability density functions (PDFs) of daily SAT anomalies associated with North Pacific blocking events. (a–h) Probability density functions (PDFs) of daily SAT ($SAT_A = SAT_B - SAT_M$) anomalies averaged over the western (120° – 100° W, 40° – 60° N) and Eastern (80° – 60° W, 35° – 55° N) North America from lag -10 to 10 days during the life cycles of North Pacific blocking (PB) events for (a, e) PDO^- & AMO^- , (b, f) PDO^- & AMO^+ , (c, g) PDO^+ & AMO^- and (d, h) PDO^+ & AMO^+ combinations based on the above definitions in terms of 9–30-year band-pass filtered PDO index and 30-year low-pass filtered AMO index, where SAT_M denotes the time-mean value of daily SAT (SAT_B) anomalies of all blocking days of all PB events from lag-10 to 10 days. The red line represents a fitted curve, whereas μ_{PB} represents the mean value of SAT anomalies for each case.

strong widespread cold anomaly is still formed over all of North America (Figure 3e) because AMO^- favors NAO^+ events (Li et al., 2013). Although we see a sub-seasonal WWCE dipole for PDO^+ & AMO^- and PDO^+ & AMO^+ (Figures 3g and 3h), the PB can cause a sub-seasonal cold west-warm east (CWWE) dipole, a reversal dipole of the WWCE regime, due to the joint role of PB and NAO^- events in the PDO^- & AMO^+ winter (Figure 3f). The reason for this is that the AMO^+ is favorable for NAO^- events that lead to warm anomalies over the eastern North American mid-high latitudes. Thus, the different combinations of AMO^+ with PDO^+ and PDO^- over 1998–2022 can regulate the decadal shift of North American temperature extreme patterns via decadal changes in PB events.

3.5. Integrative Effects of North Pacific Blocking Events on Shaping the Decadal SAT Variability

Finally, in Figure 4 we have defined $SAT_A(t) = SAT_B(t) - SAT_M$, where SAT_B is the daily SAT anomaly during the lifecycle from lag -10 to 10 days for each blocking event, and SAT_M is the mean SAT anomaly for all blocking days of 166 PB events in a given region. The probability distribution function (PDF) of daily SAT anomaly during the blocking lifecycle, as shown in Figure 4, shows that the mean SAT associated with PB events is shifted to a strong cold (weak warm) anomaly in western North America (Figures 4b and 4d), but a strong warm (weak cold) anomaly in eastern North America (Figures 4f and 4h) under PDO^- & AMO^+ (PDO^+ & AMO^+). Thus, the PB can induce a weak sub-seasonal WWCE dipole for PDO^+ & AMO^+ over 1990–2022 partly because the PDO^+ has a smaller mean amplitude over 1990–2022 than over 1950–1989 when the AMO index increases and shifts toward a positive phase over 1990–2022. In contrast, the PB can cause a stronger sub-seasonal CWWE dipole for PDO^-

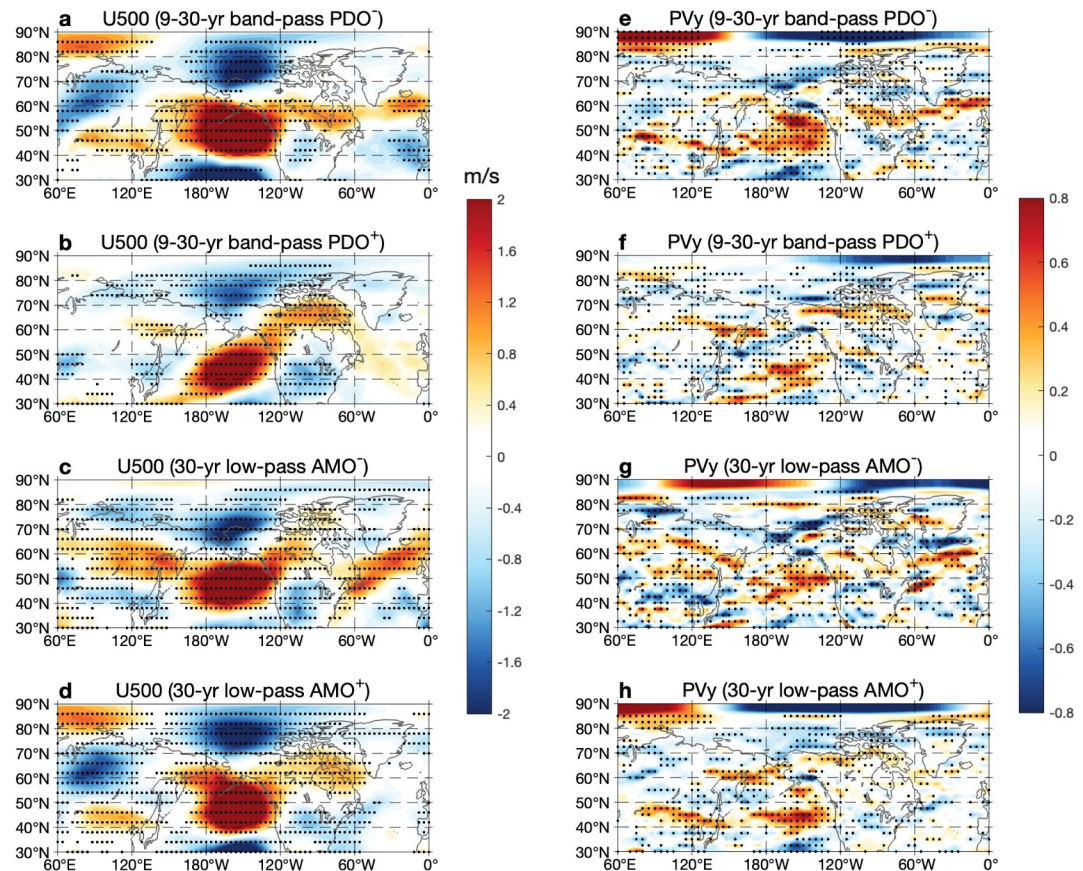


Figure 5. Spatial patterns of composite winter 500-hPa zonal wind (U500) and meridional potential vorticity gradient (PV_y or PV_y) anomalies for the different phases of PDO and AMO: (a–h) Composite winter (December to February, DJF) mean 500-hPa (a–d) zonal wind (U500, color shading, in m/s) and (e–h) meridional potential vorticity gradient (PV_y, unit: non-dimensional) anomalies without North Pacific blocking (PB) events during 1950–2022 for the (a, e) negative and (b, f) positive PDO (PDO[−] and PDO⁺) as well as the (c, g) negative and (d, h) positive AMO (AMO[−] and AMO⁺) defined in terms of the 9–30-year (or 9–30-yr) band-pass PDO index and 30-year (or 30-yr) low-pass AMO index, where the case without PB events represents that the blocking days from lag −10 to 10 days (lag 0 denotes the peak day of PB) are removed for each PB event and the dot denotes the region being statistically significant at the 95% confidence level for a two-sided Student's *t*-test.

& AMO⁺ over 1990–2022 partly because the PDO[−] has larger mean amplitude over 1990–2022 than over 1950–1989. Thus, when AMO⁺ is dominant over 1990–2022, the phase shift of PDO from PDO⁺ to PDO[−] can lead to a shift from a WWCE dipole to a strong CWWE dipole. This explains why the CWWE dipole over North America has a larger mean amplitude than the WWCE dipole during 1990–2022. Because the PDO has a shorter period during 1990–2022 than during 1950–1989, a decadal alteration between the winter WWCE and CWWE dipoles is accelerated during 1990–2022.

4. Summary and Discussion

In this study, we find that winter North American SAT exhibits a decadal alternation between warm west-cold east (WWCE) and cold west-warm east (CWWE) dipoles with a shorter mean decadal period during 1990–2022 than during 1950–1989. Moreover, the WWCE (CWWE) dipole has a smaller (larger) mean amplitude during 1990–2022 than during 1950–1989. Thus, the decadal variability of the North American temperature extreme pattern, which leads to decadal changes in North American drought and wildfires in the recent decades (McCabe et al., 2004; Zhuang et al., 2021), resembles the PDO variability under greenhouse warming (Fang et al., 2014; Geng et al., 2019; Zhang & Delworth, 2016), primarily because the variability of the SAT PCI time series is similar to the PDO variability in period and amplitude. Consequently, one could infer that the decadal alteration of the winter WWCE and CWWE dipoles is accelerated during 1990–2022, which has a footprint of the PDO variability under anthropogenic warming, even though the winter WWCE or CWWE dipoles, as a result of

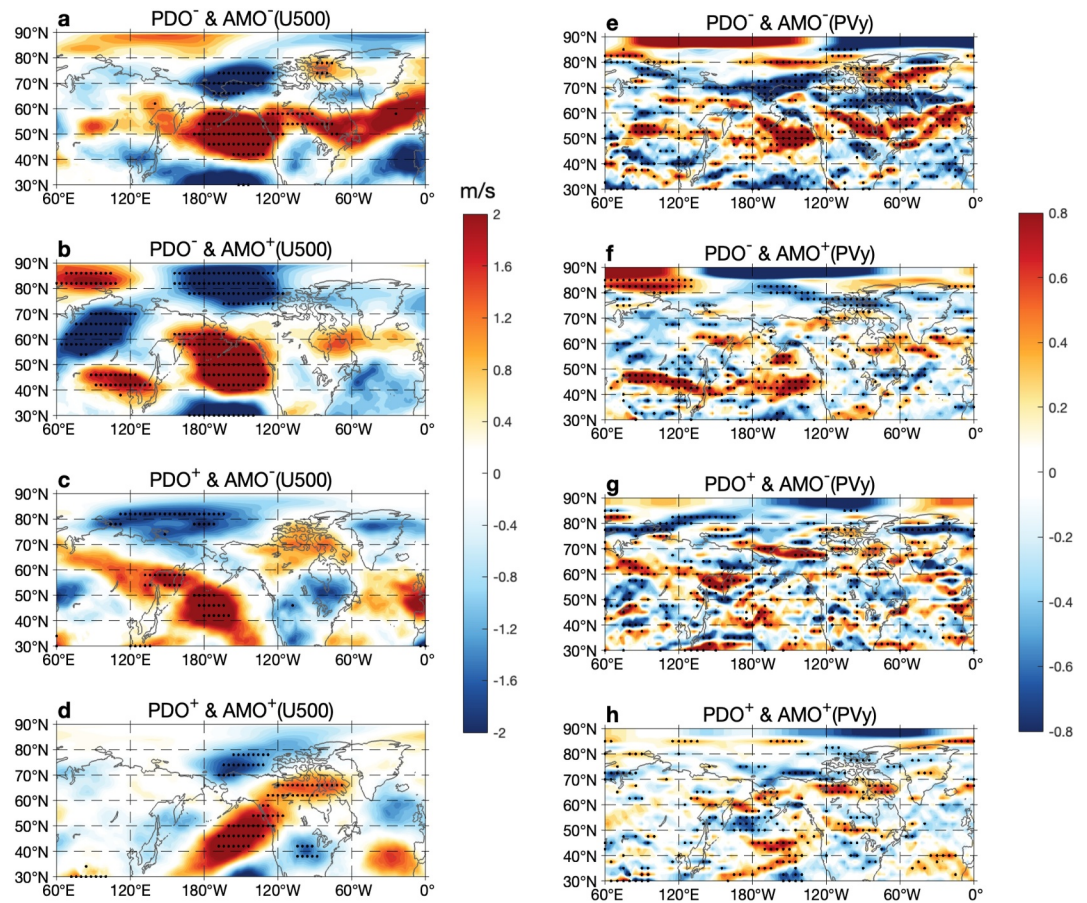


Figure 6. Same as Figure 5 but for (a, e) PDO^- & AMO^- , (b, f) PDO^- & AMO^+ , (c, g) PDO^+ & AMO^- and (d, h) PDO^+ & AMO^+ .

the winter mean sub-seasonal zonal dipoles, are mainly related to North Pacific blocking events. This reflects the indirect effect of anthropogenic warming trend. In a word, anthropogenic warming trend can significantly influence the recent decadal shift in winter North American temperature patterns via altering the PDO and its effect on North Pacific blocking. Moreover, it is further concluded that the winter WWCE or CWWE dipoles over North America will be less predictable in a future warming climate, as the predictability of the PDO variability is reduced under increasing Carbon dioxide emission scenarios (Li et al., 2020).

We also find that the winter WWCE or CWWE dipole can be considered as a result of the winter mean sub-seasonal WWCE or CWWE dipoles. The PDO^+ (PDO^-) favors a sub-seasonal warm (cold) anomaly associated with PB events in western North America via decadal changes in mean zonal winds and PV_y over North Pacific. PDO^+ tends to promote a winter WWCE dipole over North America when it coincides with AMO^+ . In contrast, a sub-seasonal CWWE dipole is favored by the PB when PDO^- coincides with AMO^+ . Since the AMO^+ winters are prevalent during 1998–2022, the transition of PDO from PDO^+ to PDO^- can induce a notable decadal shift in the winter North Atlantic SAT regimes from a sub-seasonal WWCE dipole (Figure 3h) to a sub-seasonal CWWE dipole (Figure 3f). This phase shift is more evident over 1994–2022, which has led to more frequent cold winters in western North America and warm winters in eastern North America in recent years. Such changes tend to inhibit droughts or wildfires in western North America, while promoting them in eastern North America.

It should be pointed out that greenhouse warming trend can indirectly influence the North American winter weather patterns via altering the PDO due to changes in the oceanic basic state (Fang et al., 2014; Geng et al., 2019; Li et al., 2020; Saenko, 2006; Zhang & Delworth, 2016), even though the PDO is fundamentally thought of as an internal decadal mode. The effect of the greenhouse warming trend persists in the PDO variability through changes in the PDO period and amplitude (Geng et al., 2019; Zhang & Delworth, 2016). While we have

examined the cause of the decadal variability of the winter North American weather regimes, the impact of ENSO on them and its combined effect with PDO and AMO are not considered here, but has been addressed in earlier studies (Peng et al., 2019; Ge & Luo, 2023a, 2023b; Wang et al., 2014; Zhuang et al., 2021). However, our present results significantly improve our understanding of the decadal changes in the winter North American weather regimes and enhance our knowledge regarding the management of economic activity and water resources.

Conflict of Interest

The authors declare no conflicts of interest relevant to this study.

Data Availability Statement

All data are publicly available. We used the ERA5 reanalysis of European Centre for Medium-Range Weather Forecasts (ECMWF) (available at <https://doi.org/10.24381/cds.adbb2d47>) (Hersbach et al., 2020). The ERA5-Land data (available at <https://doi.org/10.24381/cds.e2161bac>) (Muñoz-Sabater et al., 2021). The winter PDO index taken from the National Centers for Environmental Information (available at <https://www.ncei.noaa.gov/access/monitoring/pdo/>) and winter AMO index taken from Koninklijk Nederlands Meteorologisch Instituut (KNMI) Climate Explorer (available at <http://climexp.knmi.nl/selectindex.cgi?id=someone@somewhere>, under the “Atlantic Multidecadal Oscillation derived from HadSST (1850–now) SST EQ–60°N, 0°–80°W minus SST 60°S–60°N” section). All the codes used in this study are available from the first corresponding author on request or from the website (available at <https://doi.org/10.6084/m9.figshare.26489416.v3>) (Luo, 2024).

Acknowledgments

This work was supported by was supported by the National Key Research and Development Program of China (2023YFF0805101) and the National Natural Science Foundation of China (Grants: 42288101, 42150204). B. L. was supported by the National Natural Science Foundation of China (Grant 42405023), the China National Postdoctoral Program for Innovative Talents (BX20230045) and the China Postdoctoral Science Foundation (2023M730279). C. D. was supported by the Beijing Normal University Talent Introduction Project of China (12807-312232101, 2022-GJTD-01). I. S. was supported by the Australian Research Council (Grant DP 160101997). X. Z. was supported by the US Department of Energy (DOE) grant #DE-SC0024872, the DOE's National Energy Research Scientific Computing Center (NERSC) project m4622, and the US NOAA CISSS Agreement #NA24NESX432C0001T101.

References

- Abolafia-Rosenzweig, R., He, C., & Chen, F. (2022). Winter and spring climate explains a large portion of interannual variability and trend in western US summer fire burned area. *Environmental Research Letters*, *17*(5), 054030. <https://doi.org/10.1088/1748-9326/ac6886>
- Cohen, J., Agel, L., Barlow, M., & Entekhabi, D. (2023). No detectable trend in mid-latitude cold extremes during the recent period of Arctic amplification. *Communications Earth and Environment*, *4*(1), 341. <https://doi.org/10.1038/s43247-023-01008-9>
- Considine, T. J. (2000). The impacts of weather variations on energy demand and carbon emissions. *Resource and Energy Economics*, *22*(4), 295–314. [https://doi.org/10.1016/S0928-7655\(00\)00027-0](https://doi.org/10.1016/S0928-7655(00)00027-0)
- Dai, A. (2013). The influence of the inter-decadal Pacific oscillation on US precipitation during 1923–2010. *Climate Dynamics*, *41*(3), 633–646. <https://doi.org/10.1007/s00382-012-1446-5>
- Donovan, V. M., Crandall, R., Fill, J., & Wonkka, C. L. (2023). Increasing large wildfire in the eastern United States. *Geophysical Research Letters*, *50*(24), e2023GL107051. <https://doi.org/10.1029/2023GL107051>
- Emery, W. J., & Thomson, R. E. (2004). *Data analysis methods in physical oceanography* (2d ed., pp. 533–539). Elsevier.
- Fang, C., Wu, L., & Zhang, X. (2014). The impact of global warming on the Pacific Decadal Oscillation and the possible mechanism. *Advances in Atmospheric Sciences*, *31*(1), 118–130. <https://doi.org/10.1007/s00376-013-2260-7>
- Ge, Y., & Luo, D. (2023a). Impacts of the different types of El Niño and PDO on the winter sub-seasonal North American zonal temperature dipole via the variability of positive PNA events. *Climate Dynamics*, *60*(5), 1397–1413. <https://doi.org/10.1007/s00382-022-06393-z>
- Ge, Y., & Luo, D. (2023b). Winter cold extremes over the eastern North America: Pacific origins of interannual-to-decadal variability. *Environmental Research Letters*, *18*(5), 054006. <https://doi.org/10.1088/1748-9326/accc49>
- Geng, T., Yang, Y., & Wu, L. (2019). On the mechanisms of Pacific decadal oscillation modulation in a warming climate. *Journal of Climate*, *32*(5), 1443–1459. <https://doi.org/10.1175/JCLI-D-18-0337.1>
- Hartmann, D. L. (2015). Pacific sea surface temperature and the winter of 2014. *Geophysical Research Letters*, *42*(6), 1894–1902. <https://doi.org/10.1002/2015GL063083>
- Hersbach, H., Bell, B., Berrisford, P., Hirahara, S., Horányi, A., Muñoz-Sabater, J., et al. (2020). The ERA5 global reanalysis [Dataset]. *Quarterly Journal of the Royal Meteorological Society*, *146*(730), 1999–2049. <https://doi.org/10.1002/qj.3803>
- Ji, K., Yu, J. Y., Li, J., Hu, Z. Z., Tseng, Y. H., Shi, J., et al. (2024). Enhanced North Pacific Victoria mode in a warming climate. *npj Climate and Atmospheric Science*, *7*(1), 49. <https://doi.org/10.1038/s41612-024-00599-0>
- Kug, J. S., Jeong, J. H., Jang, Y. S., Kim, B. M., Folland, C. K., Min, S. K., & Son, S. W. (2015). Two distinct influences of Arctic warming on cold winters over North America and East Asia. *Nature Geoscience*, *8*(10), 759–762. <https://doi.org/10.1038/ngeo2517>
- Kushnir, Y., & Lau, N. C. (1992). The general circulation model response to a North Pacific SST anomaly: Dependence on time scale and pattern polarity. *Journal of Climate*, *5*(4), 271–283. [https://doi.org/10.1175/1520-0442\(1992\)005<0271:TGCMRT>2.0.CO;2](https://doi.org/10.1175/1520-0442(1992)005<0271:TGCMRT>2.0.CO;2)
- Ladwig, L. M., Ratajczak, Z. R., Ocheltree, T. W., Hafich, K. A., Churchill, A. C., Frey, S. J. K., et al. (2016). Beyond arctic and alpine: The influence of winter climate on temperate ecosystems. *Ecology*, *97*(2), 372–382. <https://doi.org/10.1890/15-0153.1>
- Lee, M. Y., Hong, C. C., & Hsu, H. H. (2015). Compounding effects of warm sea surface temperature and reduced sea ice on the extreme circulation over the extratropical North Pacific and North America during the 2013–2014 boreal winter. *Geophysical Research Letters*, *42*(5), 1612–1618. <https://doi.org/10.1002/2014GL062956>
- Li, J., Sun, C., & Jin, F. F. (2013). NAO implicated as a predictor of Northern Hemisphere mean temperature multidecadal variability. *Geophysical Research Letters*, *40*(20), 5497–5502. <https://doi.org/10.1002/2013GL057877>
- Li, S., Wu, L., Yang, Y., Geng, T., Cai, W., Gan, B., et al. (2020). The Pacific Decadal Oscillation less predictable under greenhouse warming. *Nature Climate Change*, *10*(1), 30–34. <https://doi.org/10.1038/s41558-019-0663-x>
- Lin, H. (2015). Subseasonal variability of North American wintertime surface air temperature. *Climate Dynamics*, *45*(5–6), 1137–1155. <https://doi.org/10.1007/s00382-014-2363-6>
- Liu, Y., Feng, S., Qian, Y., Huang, H., & Berg, L. K. (2023). How do North American weather regimes drive wind energy at the sub-seasonal to seasonal timescales? *npj Climate and Atmospheric Science*, *6*(1), 100. <https://doi.org/10.1038/s41612-023-00403-5>

- Luo, B. (2024). Code for "Recent accelerated decadal shift in winter North American temperature patterns under Pacific-Atlantic decadal variability" [Software]. *figshare*. <https://doi.org/10.6084/m9.figshare.26489416.v3>
- Luo, B., Luo, D., Dai, A., Simmonds, I., & Wu, L. (2020). Combined influences on North American winter air temperature variability from North Pacific blocking and the North Atlantic Oscillation: Subseasonal and interannual time scales. *Journal of Climate*, 33(16), 7101–7123. <https://doi.org/10.1175/JCLI-D-19-0327.1>
- Luo, D., & Zhang, W. (2020). A nonlinear multiscale theory of atmospheric blocking: Dynamical and thermodynamic effects of meridional potential vorticity gradient. *Journal of the Atmospheric Sciences*, 77(7), 2471–2500. <https://doi.org/10.1175/JAS-D-20-0004.1>
- Luo, D., Zhang, W., Zhong, L., & Dai, A. (2019). A nonlinear theory of atmospheric blocking: A potential vorticity gradient view. *Journal of the Atmospheric Sciences*, 76(8), 2399–2427. <https://doi.org/10.1175/JAS-D-18-0324.1>
- McCabe, G. J., Palecki, M. A., & Betancourt, J. L. (2004). Pacific and Atlantic Ocean influences on multidecadal drought frequency in the United States. *Proceedings of the National Academy of Sciences*, 101(12), 4136–4141. <https://doi.org/10.1073/pnas.0306738101>
- Mo, K. C., Schemm, J. K. E., & Yoo, S. H. (2009). Influence of ENSO and the Atlantic Multidecadal Oscillation on drought over the United States. *Journal of Climate*, 22(22), 5962–5982. <https://doi.org/10.1175/2009JCLI2966.1>
- Muñoz-Sabater, J., Dutra, E., Agustí-Panareda, A., Albergel, C., Arduini, G., Balsamo, G., et al. (2021). ERA5-Land: A state-of-the-art global reanalysis dataset for land applications [Dataset]. *Earth System Science Data*, 13(9), 4349–4383. <https://doi.org/10.5194/essd-13-4349-2021>
- North, G. R., Bell, T. L., Cahalan, R. F., & Moeng, F. J. (1982). Sampling errors in the estimation of empirical orthogonal functions. *Monthly Weather Review*, 110(7), 699–706. [https://doi.org/10.1175/1520-0493\(1982\)110<0699:SEITEO>2.0.CO;2](https://doi.org/10.1175/1520-0493(1982)110<0699:SEITEO>2.0.CO;2)
- Overland, J. E., Wood, K. R., & Wang, M. (2011). Warm Arctic—Cold continents: Climate impacts of the newly open Arctic Sea. *Polar Research*, 30(1), 15787. <https://doi.org/10.3402/polar.v30i0.15787>
- Peng, P., Kumar, A., Chen, M., Hu, Z. Z., & Jha, B. (2019). Was the North American extreme climate in winter 2013/14 a SST forced response? *Climate Dynamics*, 52(5–6), 3099–3110. <https://doi.org/10.1007/s00382-018-4314-0>
- Pitcher, E. J., Blackmon, M. L., Bates, G. T., & Muñoz, S. (1988). The effect of North Pacific sea surface temperature anomalies on the January climate of a general circulation model. *Journal of the Atmospheric Sciences*, 45(2), 173–188. [https://doi.org/10.1175/1520-0469\(1988\)045<0173:TEONPS>2.0.CO;2](https://doi.org/10.1175/1520-0469(1988)045<0173:TEONPS>2.0.CO;2)
- Saenko, O. A. (2006). Influence of global warming on baroclinic Rossby radius in the ocean: A model intercomparison. *Journal of Climate*, 19(7), 1354–1360. <https://doi.org/10.1175/JCLI3683.1>
- Singh, D., Swain, D. L., Mankin, J. S., Horton, D. E., Thomas, L. N., Rajaratnam, B., & Diffenbaugh, N. S. (2016). Recent amplification of the North American winter temperature dipole. *Journal of Geophysical Research: Atmospheres*, 121(17), 9911–9928. <https://doi.org/10.1002/2016JD025116>
- Smith, E. T., & Sheridan, S. C. (2018). The characteristics of extreme cold events and cold air outbreaks in the eastern United States. *International Journal of Climatology*, 38(S1), e807–e820. <https://doi.org/10.1002/joc.5408>
- Swain, D. L., Horton, D. E., Singh, D., & Diffenbaugh, N. S. (2016). Trends in atmospheric patterns conducive to seasonal precipitation and temperature extremes in California. *Science Advances*, 2(4), e1501344. <https://doi.org/10.1126/sciadv.1501344>
- Tibaldi, S., & Molteni, F. (1990). On the operational predictability of blocking. *Tellus*, 42(3), 343–365. <https://doi.org/10.3402/tellusa.v42i3.11882>
- Vavrus, S., Walsh, J. E., Chapman, W. L., & Portis, D. (2006). The behavior of extreme cold air outbreaks under greenhouse warming. *International Journal of Climatology: A Journal of the Royal Meteorological Society*, 26(9), 1133–1147. <https://doi.org/10.1002/joc.1301>
- Veres, M., & Hu, Q. (2015). Atmospheric responses to North Atlantic SST anomalies in idealized experiments. Part I: Northern Hemispheric circulation. *Journal of Climate*, 28(15), 6204–6220. <https://doi.org/10.1175/JCLI-D-14-00413.1>
- Vigaud, N., Robertson, A. W., & Tippett, M. K. (2018). Predictability of recurrent weather regimes over North America during winter from submonthly reforecasts. *Monthly Weather Review*, 146(8), 2559–2577. <https://doi.org/10.1175/MWR-D-18-0058.1>
- Walsh, J. E., Phillips, A. S., Portis, D. H., & Chapman, W. L. (2001). Extreme cold outbreaks in the United States and Europe, 1948–99. *Journal of Climate*, 14(12), 2642–2658. [https://doi.org/10.1175/1520-0442\(2001\)014<2642:ECOITU>2.0.CO;2](https://doi.org/10.1175/1520-0442(2001)014<2642:ECOITU>2.0.CO;2)
- Wang, S. Y., Hippias, L., Gillies, R. R., & Yoon, J. (2014). Probable causes of the abnormal ridge accompanying the 2013–2014 California drought: ENSO precursor and anthropogenic warming footprint. *Geophysical Research Letters*, 41(9), 3220–3226. <https://doi.org/10.1002/2014GL059748>
- Wang, S. Y. S., Yoon, J. H., Becker, E., & Gillies, R. (2017). California from drought to deluge. *Nature Climate Change*, 7(7), 465–468. <https://doi.org/10.1038/nclimate3330>
- Wilks, D. S. (2011). *Statistical methods in the atmospheric sciences* (3rd ed.). Academic Press.
- Yu, B., Lin, H., Wu, Z. W., & Merryfield, W. J. (2016). Relationship between North American winter temperature and large-scale atmospheric circulation anomalies and its decadal variation. *Environmental Research Letters*, 11(7), 074001. <https://doi.org/10.1088/1748-9326/11/7/074001>
- Yu, B., & Zhang, X. (2015). A physical analysis of the severe 2013/2014 cold winter in North America. *Journal of Geophysical Research: Atmospheres*, 120(19), 10149–10165. <https://doi.org/10.1002/2015JD023116>
- Zhang, L., & Delworth, T. L. (2016). Simulated response of the Pacific decadal oscillation to climate change. *Journal of Climate*, 29(16), 5999–6018. <https://doi.org/10.1175/JCLI-D-15-0690.1>
- Zhang, R., Screen, J. A., & Zhang, R. (2022). Arctic and Pacific Ocean conditions were favorable for cold extremes over Eurasia and North America during winter 2020/21. *Bulletin of the American Meteorological Society*, 103(10), E2285–E2301. <https://doi.org/10.1175/BAMS-D-21-0264.1>
- Zhang, W., Hari, V., Wang, S., LaPlante, M. D., Garfin, G., Afram, G., & Kumar, R. (2022). Fewer troughs, not more ridges, have led to a drying trend in the Western United States. *Geophysical Research Letters*, 49(1), e2021GL097089. <https://doi.org/10.1029/2021GL097089>
- Zhang, W., & Luo, D. (2020). A nonlinear theory of atmospheric blocking: An application to Greenland blocking changes linked to winter Arctic sea ice loss. *Journal of the Atmospheric Sciences*, 77(2), 723–751. <https://doi.org/10.1175/JAS-D-19-0198.1>
- Zhang, X., Fu, Y., Han, Z., Overland, J. E., Rinke, A., Tang, H., et al. (2022). Extreme cold events from East Asia to North America in winter 2020/21: Comparisons, causes, and future implications. *Advances in Atmospheric Sciences*, 39(4), 553–565. <https://doi.org/10.1007/s00376-021-1229-1>
- Zhuang, Y., Fu, R., Santer, B. D., Dickinson, R. E., & Hall, A. (2021). Quantifying contributions of natural variability and anthropogenic forcings on increased fire weather risk over the western United States. *Proceedings of the National Academy of Sciences of the United States of America*, 118(45), e2111875118. <https://doi.org/10.1073/pnas.2111875118>
- Zou, Y., Rasch, P. J., Wang, H., Xie, Z., & Zhang, R. (2021). Increasing large wildfires over the western United States linked to diminishing sea ice in the Arctic. *Nature Communications*, 12(1), 6048. <https://doi.org/10.1038/s41467-021-26232-9>